Study of fibrinogen adsorption on poly(ethylene glycol)-modified surfaces using a quartz crystal microbalance with dissipation and a dual polarization interferometry

ARTICLE *in* RSC ADVANCES · JANUARY 2014

Impact Factor: 3.84 · DOI: 10.1039/C3RA46934D

RSC Advances

PAPER

View Article Online
View Journal | View Issue

Cite this: *RSC Adv.*, 2014, **4**, 7716

Study of fibrinogen adsorption on poly(ethylene glycol)-modified surfaces using a quartz crystal microbalance with dissipation and a dual polarization interferometry

Yu Hu,[ab] Jing Jin,*[a] Yuanyuan Han,[a] Jinghua Yin,[a] Wei Jiang*[a] and Haojun Liang[c]

Received 22nd November 2013
Accepted 7th January 2014

DOI: 10.1039/c3ra46934d

www.rsc.org/advances

Protein adsorption behavior is a key factor that determines whether materials can be used as medical polymer materials. In this study, fibrinogen (Fib) adsorptions on three different poly(ethylene glycol) (PEG) surfaces that differed in chain length and chain density were investigated using a quartz crystal microbalance with dissipation (QCM-D) and a dual polarization interferometry (DPI) with respect to adsorbed masses, viscoelastic properties and chain conformations. On QCM-D chips, PEG chains were tight and in extended brush conformations. Meanwhile, on DPI chips, PEG_{1000} and PEG_{2000} may have the same pancake-like conformations, but PEG_{5000} had a mushroom conformation. Moreover, several bare spaces were observed on the loose pancake-like PEG_{1000}- and PEG_{2000}-modified DPI surfaces. Fib could fully spread on the relatively dense PEG_{1000}-modified DPI surface and partly spread and tightly orient on the relatively sparse PEG_{2000}-modified DPI surface. Thus, grafting density was found to have greater significance in determining Fib adsorption resistance due to its influence on Fib spreading when the chain conformations of hydrophilic molecules were loose pancake-like structures. Furthermore, brush and mushroom structured PEG_{5000} chains both had high deformation capacity, which excellently resisted protein adsorption by adjusting their conformation to decrease interaction with Fib. Therefore, the Fib adsorption resistance of PEG-modified surface depended on the grafting density of PEG layer and the deformation capacity of the PEG chain.

1. Introduction

Plasma protein adsorption from blood plasma is a key factor that determines whether materials can be used as medical polymer materials. Fibrinogen (Fib) is an adhesive protein with a rodlike structure (47 nm × 5 nm × 5 nm)[1,2] and plays a vital role in coagulation, platelet activation and aggregation, inflammatory response, and leucocyte binding. The Fib molecule consists of two peripheral D domains and one central E domain held together by triple-stranded α-helical coiled coils (Fig. 1). Paul *et al.*[3] found that the positively charged αC domains may play a role in keeping Fib soluble in the blood stream, which could inhibit blood coagulation. Therefore, understanding the Fib adsorption behavior and mechanism at polymer surface is significant for fabricating high performance blood-contacting materials.[4]

Fib adsorptions on various substrates have been extensively studied.[5] The adsorption on polymer surface is a complex process. It involves van der Waals forces, hydrophobic interactions, electrostatic interactions, and hydrogen bonding[6,7] and depends on the chemical and physical characteristics of the

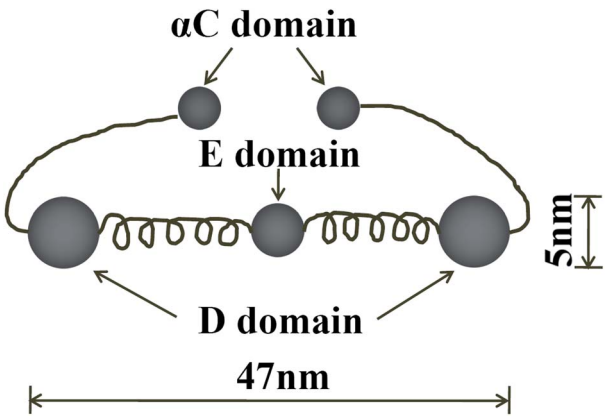

Fig. 1 Schematic diagram shows the structure of fibrinogen.

[a]*State Key Laboratory of Polymer Physics and Chemistry, Changchun Institute of Applied Chemistry, Chinese Academy of Sciences, Changchun 130022, PR China. E-mail: wjiang@ciac.ac.cn; jjin@ciac.ac.cn; Fax: +86-431-85262126; Tel: +86-431-85262151*

[b]*Graduate University of Chinese Academy of Sciences, Beijing 100049, PR China*

[c]*CAS Key Laboratory of Soft Matter Chemistry, Department of Polymer Science and Engineering, University of Science and Technology of China, Hefei, Anhui 230026, PR China*

surface, such as hydrophilicity, densities, conformations, and orientations of surface polymer chains.[8] Zbigniew Adamczyk *et al.* performed systematic studies on Fib adsorption on polystyrene (PS) latex particles. They proposed a robust procedure of preparing Fib monolayer on the PS surface of well-controlled orientation and coverage for immunological assays[9] and presented two main adsorption mechanisms of Fib, namely, the random and the side-on adsorption mechanisms.[10] However, a few working about mechanism of Fib adsorption on the hydrophilic polymer surface, such as poly (ethylene glycol) (PEG)-modified surface, has been conducted.[11] PEG is a nontoxic and nonimmunogenic polymer that possesses excellent protein resistant property.[12] Moreover, PEG is also commonly used to induce protein crystallization.[13] PEG layer density, chain length and chain conformation[14] are important factors affecting the protein resistant of the PEG layer.[15,16] Although the interactions between Fib and PEG-modified surface have been studied for many years,[17–19] the dynamic interaction mechanism in the molecular level of resistance of PEG against Fib adsorption is yet to be clarified.

Currently, some new techniques, such as ellipsometry,[20] total internal reflection fluorescence,[21] quartz crystal microbalance with dissipation (QCM-D),[22,23] and surface plasmon resonance[24] are used to probe the interaction between protein and polymer surface. However, the protein needs to be labeled in some of these techniques, and the information obtained by using these techniques individually is limited. As a result, the dynamic interaction between protein and surface can hardly be elucidated in the molecular level. Additionally, only a few studies have investigated the quantitative structure–property relationships between protein and surface from the perspective of protein denaturing and orientation changes.[25] Therefore, a combination of QCM-D and other techniques, such as dual polarization interferometry (DPI), ellipsometry,[26] neutron reflectivity, and high-energy X-ray reflectivity[27] is imperative for the investigation of protein adsorption on polymer surface. Based on the inverse piezoelectric effect of piezoelectric quartz crystal, QCM-D is a powerful tool for examining the tiny mass variation on crystal surface and the viscoelasticity property of the adsorbed layer simultaneously in real-time.[28] Meanwhile, DPI is a surface sensitive technique for the real-time monitoring of the interaction in the solid–liquid interface, which can simultaneously obtain the changes in layer mass, thickness, and density.[29] Several groups have studied the interaction between biomacromolecules and interface and surface properties using these two techniques.[26,30–32] Kairuo Xu *et al.*[33] investigated lysozyme adsorption on a silica surface by combining these two techniques in parallel and proposed a tentative lysozyme adsorption model.

In the present study, both QCM-D and DPI were performed in a parallel manner to investigate the process of thiolated (SH–) monomethoxy PEG (mPEG) immobilization as well as the interaction between PEG modified surfaces and Fib. PEG-modified surfaces were fabricated with different molecular weights. The SH-mPEG chains and Fib adsorption processes on the different modified surfaces were monitored with QCM-D and DPI. The dynamic variation of the adsorbed layer properties were recorded in real-time. This study aims to provide a new understanding of the Fib adsorption on the PEG layer from another perspective and elucidate the key factors to obtain an effective protein-resistant PEG-modified surface.

2. Materials and methods

2.1 Materials

Fibrinogen (F8630), (3-aminopropyl)triethoxysilane (98%), Hellmanex™II were obtained from Sigma Chemical Co. Thiolated monomethoxy poly (ethylene glycol) (mPEG-SH) (M_w 1000, M_w 2000, M_w 5000) were obtained from shanghai Yare Biotech Inc. (Shanghai, China). Phosphate-buffered saline (PBS 0.9% NaCl, 0.01 M phosphate buffer, pH 7.4) solution was prepared freshly. *N*-(γ-Maleimidobutyryloxy)sulfosuccinimide ester (Sulfo-GMBS) was obtained from Thermo Scientific Inc. All other reagents were analytical reagent grade and used without further purification.

2.2 Quartz crystal microbalance with dissipation (QCM-D)

QCM-D procedure was performed to record the grafting process of mPEG-SH to gold sensor surface and the Fib adsorption process (QCM-D E4, Q-sense AB, Gothenburg, Sweden). The AT-cut piezoelectric quartz crystal disks coated with gold used as the QCM-D sensor chips (Q-sense-Biolin Scientific AB, Sweden) had the fundamental frequency of 4.95 MHz and vibrate in the thickness-shear mode with the overtone *n* of 1, 3, 5, 7, 9, 11, and 13. QCM-D chip was exposed to UV-lamp (185 nm + 254 nm) for 15 min to remove organic contaminants, and then was cleaned in a 5 : 1 : 1 (v/v) solution of deionized water, ammonia (25%) and hydrogen peroxide (30%) for 5 min at 75 °C. After excessive rinsing with deionized water, the chip was blown dried with high purity nitrogen.[34] Before our experiment, the instrument channel was cleaned using Hellmanex™II diluted solution (2%, in deionized water, v/v) at a flow rate of 30 μL min^{-1} for 10 h and followed by deionized water at a flow rate of 500 μL min^{-1} for 2 h to eliminate any contaminant of the instrument. In QCM-D experiment, the temperature was controlled at 20 °C (±0.02 °C) and the flow rate was fixed at 100 μL min^{-1}. The concentration of mPEG-SH in PBS buffer was fixed at 0.2 mM, and the concentration of Fib solution was 0.01, 0.1, and 1 mg mL^{-1}, respectively. Notably, in every solution changing procedure, the pump was stopped to prevent any air injecting in.

The change of adsorbed mass produced shifts of the frequency and the viscoelasticity variation of the adsorbed layer could induce the dissipation variation. The principle of QCM-D is based on the inverse piezoelectric effect of piezoelectric quartz crystal. When the crystal was exposed to a sinusoidal electric field, a shear oscillation could be induced at the resonance frequency and the crystal's oscillation frequency decreased if an increase in mass bound to the quartz surface.[35–37] For a flat, uniform, and rigid adsorbed layer, frequency shift is proportional to the change in the adsorbed mass, and Sauerbrey relation can be used to calculate the adsorbed mass.[38]

$$\Delta M = -C\Delta f/n \quad (1)$$

where ΔM represents the adsorbed mass per unit, C is the mass sensitivity constant (17.7 ng cm^{-2} Hz^{-1}), n is the overtone number. However, if the adsorbed layer is not rigid and/or too thick, it will result in a high dissipation shift. In this situation, frequency shift will not proportional to the change of adsorbed mass. Sauerbrey relation to calculate the adsorbed mass could underestimate the actual mass. Thus, it is necessary to use the Voigt model to calculate the mass and thickness of viscoelastic layer.[39] Voigt model is a common model to be used to describe the polymer's viscoelasticity property. The model contains a spring and a dashpot as its elements to represent the elastic (storage) and inelastic (damping) behavior of a material, respectively.[40] Using this model in our fitting process, each layer is represented by four unknown parameters: layer density ρ (kg m^{-3}), layer viscosity η (or G''/ω, kg ms^{-1}), layer shear modulus μ (or G', Pa) and layer thickness σ (m).[37] The frequency shift Δf and the dissipation shift ΔD recording by QCM-D real-time have the relationship with those parameters as follows:[41,42]

$$\Delta f = f_1(n,\eta_f,\rho_f,\mu_f,\sigma_f) \quad (2)$$

$$\Delta D = f_2(n,\eta_f,\rho_f,\mu_f,\sigma_f) \quad (3)$$

$$G^* = G' + jG'' = \mu + j2\pi f\eta \quad (4)$$

In our fitting process, overtones n = 3, 5, 7, 9, 11, 13 were used, allowing the model to fit the data and calculate the four unknown parameters (η,ρ,μ,σ) by iterating using QTools software (Q-Sense). Adsorbed layer density was assumed as 1200 kg m^{-3} (consider the layer density value between the banding water density 1000 kg m^{-3} and protein density 1400 kg m^{-3}).[43] The density and viscosity of the liquid phase were set as 1000 kg m^{-3} and 0.001 kg ms^{-1}, respectively. The density of the each layer was iterated to find a suitable value then fixed in. The parameters of the layer viscosity, layer shear modulus and layer thickness were set in the range of 0.0001–0.1 kg ms^{-1}, 1×10^5 to 1×10^7 Pa, 1×10^{-11} to 1×10^{-6} m, respectively.[44]

2.3 Dual polarization interferometry (DPI)

DPI experiment was conducted using an Analight Bio200®DPI (Farfield Group Ltd., Creve, UK). Amino chip was used during the DPI experiment. The unmodified chip (Farfield Unmodified Ana Chip™ Plus) was firstly incubated in piranha solution (98 wt% concentrated sulfuric acid and 30% hydrogen peroxide with the volume ratio of 7 : 3) for 30 min at 80 °C. Afterward, the chip was rinsed with ultrapure water and blown dry with high purity nitrogen. The amino chip was obtained by silanizing the silica chip. The cleaned silica chip was immersed in the 4% (v/v) (3-aminopropyl) triethoxysilane/isopropanol solution for 2 h at room temperature, and then rinsed with isopropanol excessively. After being blown dried with high purity nitrogen, the chip was baked in oven at 120 °C for 30 min. After this, amino-modified chip was obtained.[45]

Amino-modified chip was loaded into the instrument and each chip had two fluidic channels, channel 1 and channel 3, allowing two parallel experiments simultaneously. Temperature of the instrument was stabilized at 20 °C (±0.002 °C). Degassed PBS buffer was injected first at a flow rate of 50 μL min^{-1} until a stable base line was gained. Then degassed 80 wt% ethanol in water mixture was injected, followed by degassed ultrapure (UHQ) water for 10 min each at a flow rate of 50 μL min^{-1} for calibration. After this, degassed PBS buffer was injected at the same flow rate. After the base line stable again, protein adsorption experiment started to conduct. The volume of each solution injection in the following experiments was fixed at 150 μL. Firstly, degassed sulfo-GMBS/PBS solution (1 mg mL^{-1}) was injected at a flow rate of 15 μL min^{-1} for 10 min to activate the amino-modified chip, and then rinsed by PBS buffer (degassed) for 10 min. Next, a certain concentration of SH-mPEG in PBS buffer was injected at a rate of 15 μL min^{-1} for 10 min, and then rinsed by PBS to remove the physical adsorbed PEG. Different molecular weights PEG surfaces could be modified on DPI chips using the above method. Lastly, Fib in PBS buffer with three different concentrations (0.01, 0.1, and 1 mg mL^{-1}) was injected at 10 μL min^{-1} for 15 min. The loose bound Fib was removed by PBS rinsing. After experiment, instrument was cleaned by 4% (w/v) Hellmanex solution (Hellma GmbH & Co.,) for at least 2 h at a flow rate of 50 μL min^{-1}, then rinsed by 50% (w/v) isopropanol aqueous solution at 50 μL min^{-1} for at least 2 h. At last, changed the rate to 25 μL min^{-1} and cleaned the instrument overnight.

In DPI procedure, the transverse electric (TE) and transverse magnetic (TM) signals were recorded in real-time. Layer thickness and refractive index (RI) could be achieved through the analysis of AnaLight® software (AnaLight® Resolver software, version 2.1.4). Then, the adsorbed mass was obtained according to the De Feijter equation[46] as follows:

$$\rho_L = \frac{n_L - n_{buffer}}{dn/dc} \quad (5)$$

$$m_L = \rho_L \cdot \tau_L \quad (6)$$

where m_L is the layer mass per unit area (ng mm^{-2}), τ_L is the layer thickness (nm), n_L and n_{buffer} are the refractive indexes (RI) of the adsorbed layer and the bulk solution, respectively. The dn/dc is the RI increment of the protein in the bulk solution. The standard value of 0.183 cm^3 g^{-1} was used as the RI increment of protein in all calculations.[13,25]

3. Results and discussion

3.1 The characteristics of PEG-modified surfaces

Both QCM-D and DPI are performed in a parallel manner to investigate the process of SH-mPEG immobilization and the interaction between PEG modified surface and Fib. Their experiment procedures are shown in Fig. 2. SH-mPEG with different molecular weights is grafted onto QCM-D and DPI chips by thiol–Au bond and a water-soluble amine-to-sulfhydryl crosslinker sulfo-GMBS, respectively.

Table 1 presents the PEG grafting situations detected by QCM-D and DPI. The thickness of PEG on the QCM-D chips

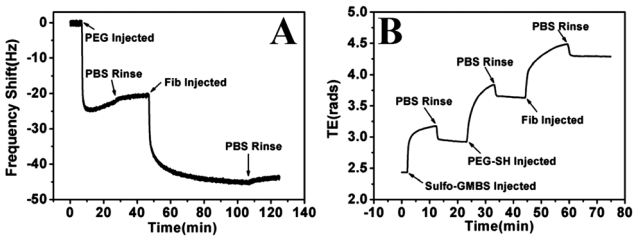

Fig. 2 The experiment procedures of (A) QCM-D and (B) DPI.

increases monotonously with PEG molecular weight, whereas its thickness on DPI chip is more complex. The thicknesses of PEG_{1000} and PEG_{2000} on DPI chips have nearly the same values, that is, 0.47 ± 0.09 nm and 0.42 ± 0.06 nm, respectively. However, the thickness of PEG_{5000} on DPI chips can reach up to 1.01 ± 0.21 nm. This result can be attributed to the difference of PEG chain conformations. The conformation of the grafted PEG chains is critical for the subsequent Fib adsorption on the modified surface. The theory work by Alexander[47] indicated that the conformation of end-tethered chains on the surface in solution depended on the grafting density Γ. However, the graft spacing S could more accurately reflect the conformations of PEG chains on QCM-D and DPI chips. The graft spacing S represents the distance between two PEG-chain attachment points, which can be derived using the following formula.

$$S = \Gamma^{(-1/2)} \quad (7)$$

Meanwhile, the hydrodynamic radius of PEG coil in solution can be reflected by Flory radius R_F as follows:

$$R_F = aN^{\nu} \quad (8)$$

where a is the ethylene oxide repeat characteristic monomer dimension and is taken as 0.278 nm, N is the degree of polymerization (the values of N is taken as 22, 45, and 113 for PEG_{1000}, PEG_{2000}, and PEG_{5000}, respectively), and ν is taken as 0.6 for high-solubility conditions.[48] When S is greater than $2R_F$, the PEG chains are more likely to be in a random coil conformation; otherwise, the PEG chains are more likely to be in an extended conformation. Moreover, the repulsive force among the chains is much stronger when the value of S is smaller. In strong repulsive force, PEG chains are more extended. When S decreases to a critical value, the grafted chains tend to be in a brush conformation.

Table 1 shows that the S values of PEG-modified QCM-D chips with three molecular weights are actually considerably smaller than their corresponding $2R_F$ values, indicating that the PEG chains on QCM-D chips are all tight and in extended brush conformations. In addition, the S values on QCM-D surfaces are smaller because the mass is the hydrated mass that contains coupled water. Fig. 3 is a schematic diagram demonstrating the chain conformation of PEG on QCM-D and DPI chips. Moreover, the PEG_{1000} layer has the largest grafting density, and the PEG_{2000} and PEG_{5000} layers have lower grafting densities on QCM-D chips. Although the S values of PEG-modified DPI chips with three molecular weights are also smaller than their corresponding $2R_F$ values, the difference between S and the corresponding $2R_F$ is relatively insignificant. Compared with the PEG-modified QCM-D chip, the chain density Γ of the PEG-modified DPI chip is relatively low. Thus, the conformations of PEG chains on DPI chips are relatively sparse and loose (Fig. 3). Furthermore, the thickness difference on the PEG-modified DPI chips indicates that PEG_{1000} and PEG_{2000} may have the same pancake-like conformations, whereas PEG_{5000} has a mushroom conformation.

3.2 The adsorbed mass of Fib determined by QCM-D and DPI

Fib adsorbed mass on QCM-D chips can be obtained by the Voigt model, and DPI measurement can directly derive the real-time Fib adsorbed mass at each concentration. Fig. 4 shows that

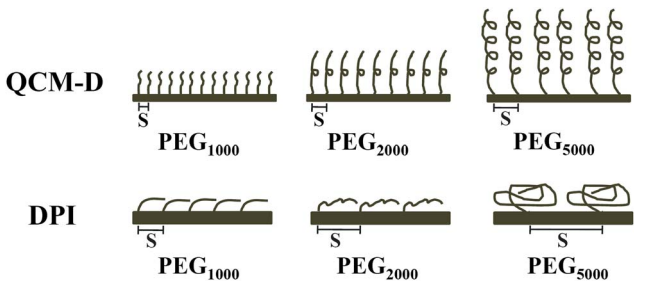

Fig. 3 Schematic diagram of PEG chain conformations on QCM-D and DPI chips.

Table 1 PEG grafting situation analysis by QCM-D and DPI

	PEG	ΔF (Hz)	$\Delta D(\times 10^{-6})$	Thickness (nm)	Γ^a (chains nm^{-2})	$S = \Gamma^{b(-1/2)}$ (nm)	$2R_F{}^c$ (nm)
QCM-D	M_w 1000	17.2 ± 3.3	0.87 ± 0.12	2.5 ± 0.4	1.81 ± 0.3	0.74	3.55
	M_w 2000	26.3 ± 1.5	0.97 ± 0.11	4.0 ± 0.2	1.51 ± 0.1	0.81	5.46
	M_w 5000	45.1 ± 1.8	1.53 ± 0.14	6.8 ± 0.3	0.99 ± 0.1	1.01	9.48
DPI	M_w 1000	—	—	0.47 ± 0.09	0.10 ± 0.01	3.16	3.55
	M_w 2000	—	—	0.42 ± 0.06	0.05 ± 0.01	4.47	5.46
	M_w 5000	—	—	1.01 ± 0.21	0.03 ± 0.01	5.77	9.48

[a] Γ is chain density. [b] S is the distance between two PEG chains attachment points. [c] R_F is Flory radius, $R_F = aN^{\nu}$, a is the ethylene oxide repeat characteristic monomer dimension and taken as 0.278 nm, N is the degree of polymerization, ν taken as 0.6 for high-solubility conditions.[48]

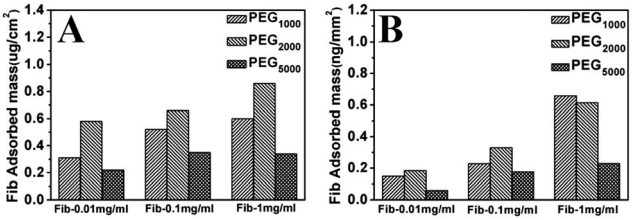

Fig. 4 Adsorbed mass of Fib at different concentrations on PEG surfaces with different molecular weights detected by (A) QCM-D and (B) DPI.

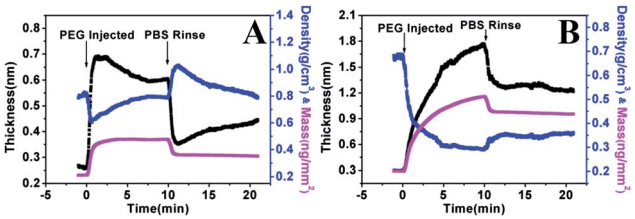

Fig. 5 Real-time DPI measurement of thickness, mass, and density during the grafting of (A) PEG_{1000} and (B) PEG_{5000}.

the Fib adsorbed mass determined by the two techniques increases with the increment of Fib concentration. In addition, the Fib adsorbed mass of the PEG_{5000}-modified surface detected by QCM-D is lower than 4 ng mm^{-2} at a flow rate of 100 μL min^{-1} for 60 min, and that detected by DPI is lower than 0.3 ng mm^{-2} at a flow rate of 10 μL min^{-1} for 15 min. Notably, PEG_{5000} has the minimum Fib adsorbed mass in different concentrations on both QCM-D and DPI chips, suggesting that PEG_{5000} can minimize the interaction between the Fib molecule and the PEG chain and resist the Fib adsorption, regardless of whether it is applied on QCM-D or DPI chips. These results also indicate that the PEG_{5000} layer possesses excellent Fib resistance, regardless of whether the PEG_{5000} chains are in brush or mushroom conformations and whether the flow rate is high or low. However, a subtle difference exists in the Fib adsorbed mass on the molecular weight dependence by the two techniques. At high concentration (1 mg mL^{-1}), the Fib adsorbed mass on the PEG_{2000}-modified QCM-D chip is larger than that of PEG_{1000}; such result is reversed on DPI chips. The dependence of adsorbed mass on molecular weight is more likely to be perturbed by flow field at high Fib concentration. The flow rates of QCM-D and DPI in our study are 100 and 15 μL min^{-1}, respectively. In addition, the van der Waals forces between PEG layer and Fib is an important factor in the Fib adsorption. The van der Waals forces due to the difference in the dispersion force between subsurface and protein affects the Fib adsorbed amounts.[49] The dispersion force on Au substrate in QCM-D and silicon substrate in DPI is 6.1 and 4.3 mN m^{-1}, respectively (the calculated results based on the contact angles of water and ethylene glycol). Thus, the tenfold difference of Fib adsorbed mass between QCM-D and DPI can be attributed to the flow rate and the van der Waals interactions.

3.3 Relationship between PEG layer viscoelasticity property and Fib adsorption

The detailed information about the grafting processes of PEG_{1000} and PEG_{5000} can be further studied by DPI. Fig. 5 shows the real-time DPI measurement results for thickness, mass, and density during the grafting of PEG_{1000} and PEG_{5000}. At the beginning of PEG_{1000} and PEG_{5000} grafting, the thickness and mass increase simultaneously. The distinct difference between PEG_{1000} and PEG_{5000} is the change of PEG layer thickness with time. Fig. 5A presents that the thickness of PEG_{1000} rapidly increases to nearly 0.7 nm. Thereafter, it slowly declines and finally reaches a stable status. The appearance of the peak in thickness can be explained by the hysteresis quality of water-soluble PEG chain. The R_F of PEG_{1000} is approximately 1.8 nm, which is less than that of PEG_{5000} (4.74 nm). The smaller Flory radius of PEG_{1000} explains why its thiol group exposed sufficiently and numerous of PEG_{1000} chains can be obtained on the chip within a short time, including grafting and physical adsorption. When the thiol terminal groups of PEG_{1000} grips onto the DPI chip, the molecule chain can be drawn in the fluid field and can then become unstable. Afterward, the PEG chains may rebound to increase their conformational entropy and maintain a more stable state. Thus, the layer thickness of PEG_{1000} decreases slowly and the density increases gradually. Finally, the thickness declines from 0.6 nm to 0.35 nm within a few seconds because the physical adsorbed PEG_{1000} is washed off. Thus, in reference to Table 1, the chain conformation of PEG_{1000} on the DPI chip has a pancake-like structure at a low grafting density. A cartoon diagram is presented in Fig. 6 to clearly illustrate this result.

Contrastingly, the PEG_{5000} layer thickness gradually increases to 1.8 nm over time. After rinsing with PBS, the PEG_{5000} layer thickness reaches up to 1.2 nm (Fig. 5B). The grafting process of PEG_{5000} onto the DPI chip is totally different from that of PEG_{1000}. The thiol terminal group of PEG_{5000} is difficult to be exposed because of the long chain entanglement and steric hindrance, leading to the time dependence of the grafting mass and thickness. As the mass of PEG_{5000} increases, the local segment–segment repulsion of PEG_{5000} accumulates and the grafting considerably slows

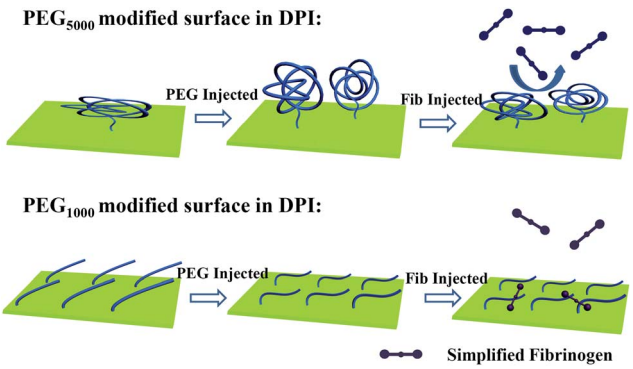

Fig. 6 Cartoon diagram of Fib adsorption on PEG_{5000} modified surface and PEG_{1000} modified surface in DPI procedure.

down. As the result of the balance between the local segment–segment repulsion and elasticity of the PEG_{5000} chains, the segments that adsorbed on the chip begin to desorb and protrude from the surface, forming additional loops and tails.[50] Finally, the conformation of PEG_{5000} on the DPI surface can form a mushroom structure.

The above analysis implies that the PEG_{1000} chains show a pancake-like conformation, whereas the PEG_{5000} chains exhibit a mushroom conformation on the DPI chips. Furthermore, PEG_{5000} has excellent Fib adsorption resistance on the DPI and QCM-D chips. We can now provide a detailed explanation by comparing the Fib adsorption process on PEG_{5000} and PEG_{1000} modified surfaces. Table 1 shows that the dissipation shift of PEG_{5000} is nearly twice as that of PEG_{1000}, suggesting that the PEG_{5000} layer has better viscoelasticity property compared to the PEG_{1000} layer. The dissipation shifts with time during the grafting of PEG_{1000} and PEG_{5000} on the QCM-D chips are shown in Fig. 7. Once the PEG_{5000} solution is injected into the QCM-D chamber, the dissipation shift rapidly increases to 3×10^{-6}. After PBS rinsing, the dissipation shift drops to 1.53×10^{-6}. However, no obvious dissipation shift is found on the PEG_{1000}-modified QCM-D chip after PBS rinsing. The larger dissipation shift on the PEG_{5000}-modified QCM-D chip can be attributed to the flexibility of longer PEG chain and larger viscoelasticity. When Fib is injected into the surface, the dissipation change of the PEG_{1000} surface becomes larger than that of PEG_{5000}. This result is because the PEG_{5000} layer possesses high deformation capacity, which can effectually reduce the interaction between the PEG chains and the Fib molecules by adjusting its conformation. Ishihara *et al.*[51] also suggested that polymer brush layers, which possessed higher elastic repulsion energies, could extremely suppress the protein–surface interactions. In other words, if a Fib molecule attempts to compress the PEG_{5000} molecule chain, a greater loss in the conformation entropy of the PEG_{5000} chain ensues because of the high deformation capacity of the PEG_{5000} chain. This entropy loss can generate a larger repulsive force between the Fib molecule and the PEG_{5000} chain. Thus, the PEG_{5000} chain with brush and mushroom structures on the QCM-D and DPI chips, respectively, both have high deformation capacity, which can resist protein adsorption excellently by adjusting its conformation to decrease the interaction with Fib.

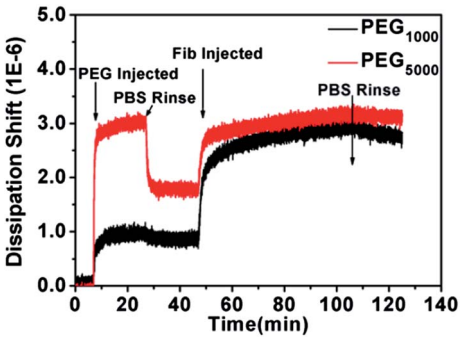

Fig. 7 Dissipation shifts with time during PEG grafting and Fib adsorption on QCM-D chips.

3.4 Relationship between PEG grafting density and Fib adsorption

Fig. 3 indicates that PEG_{1000} and PEG_{2000} have the same conformations, regardless whether they are on QCM-D or DPI chips (Table 1). PEG_{1000} and PEG_{2000} have a dense brush conformation on the QCM-D chips but have a loose pancake-like conformation on the DPI chips. In this similar conformation situation, what is the key factor that determines the final Fib adsorbed mass? Grafting density and chain length can be considered as the two most important factors.

Fib is an adhesive protein with a rod-like structure and has 47 nm × 5 nm × 5 nm dimensions. The theoretical adsorption amounts of Fib on a surface in the side-on and end-on close-packed monolayer surface coverage are 2.4 ng mm^{-2} and 22.6 ng mm^{-2}, respectively.[7] Fig. 4 reveals that all of the Fib adsorbed masses on the DPI surfaces are lower than 1.0 ng mm^{-2}. The adsorbed Fib on PEG-modified surfaces forms a monolayer. At this low-Fib surface coverage on hydrophilic surfaces, Fib is adsorbed in an elongated, less compacted manner.[52] This explanation is based on the assumption that no conformational changes occur the hydrophilic surfaces.[53] By varying PEG grafting density and Fib concentration, the Fib molecules adsorb with a different degree of spreading because of the different spaces available. Fig. 8 shows the information on the Fib adsorption on the PEG_{1000}- and PEG_{2000}-modified DPI surfaces at the concentrations of 0.1 and 1 mg mL^{-1}. At low Fib concentration (0.1 mg mL^{-1}), the thickness of Fib on the PEG_{1000}-modified surface rapidly increases to 0.8 nm, whereas that on thePEG_{2000}-modified surface increases gradually, decreases slightly after a peak 6 nm, and finally tends to be stable. By combining the dimensions of Fib and the value of the thickness variation, the orientation of adsorbed Fib can be inferred. The adsorbed Fib on the PEG_{1000}-modified surface is more likely to be in a fully spread because of the weak electrostatic interaction. This binding through positive substance and negative Fib domains can lead to a less tight binding and a higher energy loss, as shown in the dissipation in Fig. 7. Thus, the space available for the coming Fib is insufficient. However, on the PEG_{2000}-modified surface, the thickness of a monolayer Fib is 4.8 nm, which is approximate to the minor axis of Fib. Thus, the adsorbed Fib on the PEG_{2000}-modified surface may be in a side-on orientation in *z*-axis and an elongation in *x*-axis. Therefore, Fib can fully spread on the relatively dense PEG_{1000}-modified DPI surface and partly spread and tightly orient on the relatively sparse PEG_{2000}-modified DPI surface. As the Fib concentration increases to 1 mg mL^{-1}, the surface is jam-packed with Fib, and the Fib thickness on the PEG_{1000} and PEG_{2000} surfaces are 2.0 and 3.0 nm, respectively. The degree of Fib spreading decreases whereas the adsorbed amounts largely increase. Thus, due to the high Fib concentration and low surface coverage, the difference of Fib adsorbed mass between PEG_{1000} and PEG_{2000} because of the grafting density influence can be weakened.

We also compare changes of Fib adsorption rate on the PEG_{1000}- and PEG_{2000}-modified surfaces (Fig. 9) at the concentration of 0.1 mg mL^{-1}. The adsorption rate on the QCM-D chip

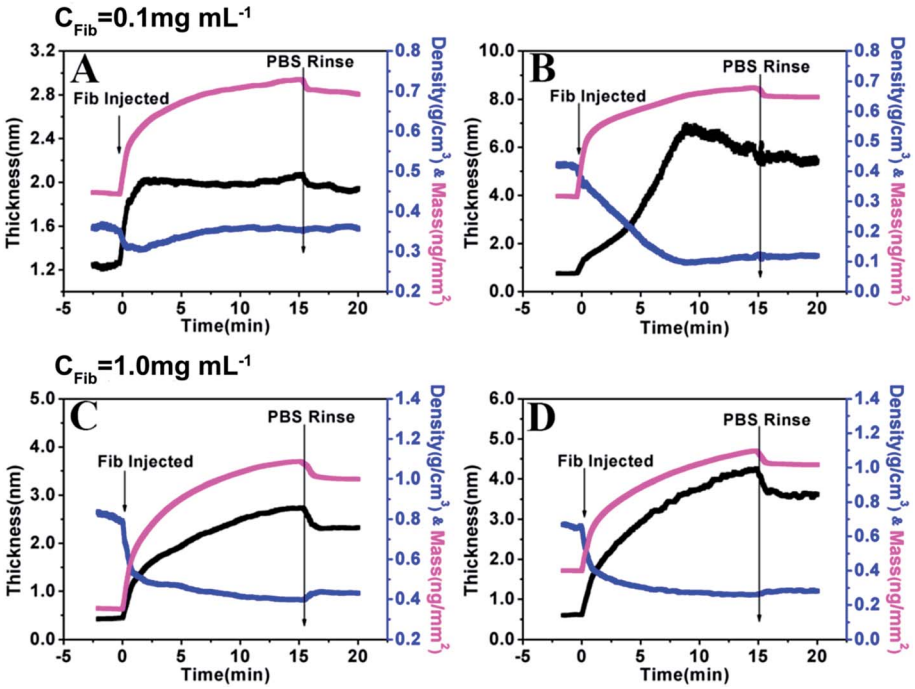

Fig. 8 Change in layer thickness and density and adsorbed mass of Fib adsorption on PEG_{1000} layer (A and C) and PEG_{2000} layer (B and D) at the concentration of 0.1 mg mL^{-1} and 1 mg mL^{-1} detected by DPI.

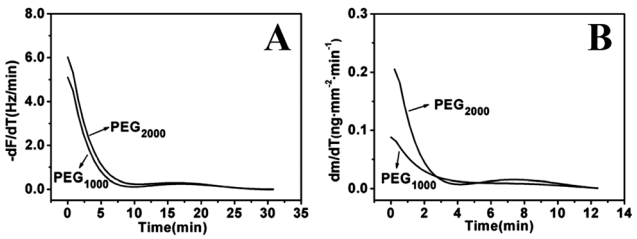

Fig. 9 Fib (0.1 mg mL^{-1}) adsorption rate on PEG_{1000} and PEG_{2000} surface detected by QCM-D (A) and DPI (B).

is taken as a derivative of the frequency with respect to time, and the rate on the DPI chip is taken as a mass derivative with respect to time. The Fib adsorption rates on the PEG_{1000}- and PEG_{2000}-modified QCM-D chips have nearly the same tendency. Actually, in the early stages of adsorption (*i.e.*, 10 min), the Fib adsorption rate on the PEG_{2000} surface is slightly faster than that of the PEG_{1000} surface at the same time. This result can be due to the high PEG grafting density of PEG_{1000} (1.81 chains nm^{-2}) compared with that of the PEG_{2000} on QCM-D chips (1.51 chains nm^{-2}). Nevertheless, a significant difference is found in the Fib adsorption rate on the PEG_{1000}- and PEG_{2000}-modified DPI chips. The Fib adsorption rate on PEG_{2000}-modified DPI chip is faster than that of on the PEG_{1000}-modified DPI chip. The adsorption rate of Fib on the PEG_{2000}-modified DPI chip quickly decreases from 0.2 ng mm^{-2} min^{-1} to zero within 4 min, whereas the rate on the PEG_{1000} modified surface changes smoothly over time. The fully spreading and elongation of Fib on the PEG_{1000} surface resists the increasing of Fib. Moreover, Table 1 shows that the conformations of PEG_{1000} and PEG_{2000} on the DPI chips have pancake-like structures, and their grafting densities are 0.10 and 0.05 chains nm^{-2}, respectively. Their thicknesses on these surfaces are both approximately 0.5 nm. In these sparse PEG-modified surfaces, the grafting density of the PEG_{1000}-modified surface is twice that of the PEG_{2000}-modified surface. This lower surface coverage for the PEG_{2000}-modified surface results in a stronger interaction with Fib compared to the PEG_{1000}-modified surface. Additional Fibs can be easily adsorbed on the PEG_{2000} surface. Furthermore, the footprint of Fib on PEG_{2000} is smaller than that on PEG_{1000}. We can conclude that the grafting density has a greater significance in determining the Fib adsorption resistance when the chain conformations of hydrophilic molecules have loose pancake-like structures. Fib could fully spread on the relatively dense PEG_{1000} layer and partly spread and tightly orient on the relatively sparse PEG_{2000} layer.

4. Conclusions

This work demonstrated the SH-mPEG with different molecular weights was grafted onto QCM-D and DPI chips by thiol–Au bond and a water-soluble amine-to-sulfhydryl crosslinker sulfo-GMBS, respectively. On QCM-D chips, PEG chains were tight and in extended brush conformations. Meanwhile, on DPI chips, PEG_{1000} and PEG_{2000} may have the same pancake-like conformations, but PEG_{5000} had a mushroom conformation.

Fib adsorptions on PEG-modified surfaces were investigated by QCM-D and DPI with respect to adsorbed masses, viscoelastic properties and chain conformations. Several bare spaces were observed on the loose pancake-like PEG_{1000}- and PEG_{2000}-

modified DPI surfaces. The adsorbed Fib on the PEG_{1000}-modified surface was more likely to be in a more elongated and fully spread because of the weak electrostatic interaction. However, the adsorbed Fib on the PEG_{2000}-modified surface may be in a side-on orientation in *z*-axis and an elongation in *x*-axis. The Fib adsorption rate on PEG_{2000}-modified DPI chip was faster than that of on the PEG_{1000}-modified DPI chip. Fib could fully spread on the relatively dense PEG_{1000}-modified DPI surface (0.10chains nm^{-2}) and partly spread and tightly orient on the relatively sparse PEG_{2000}-modified DPI surface (0.05chains nm^{-2}). Thus, grafting density was found to have greater significance in determining Fib adsorption resistance due to its influence on Fib spreading degree when the chain conformations of hydrophilic molecules were loose pancake-like structures. Furthermore, the PEG_{5000} layer possessed excellent Fib resistance, regardless of whether the PEG_{5000} chains were in brush or mushroom conformations and whether the flow rate was high or low. Both brush and mushroom structured PEG_{5000} chains had high deformation capacity, which can effectively resisted protein adsorption by adjusting their conformation to decrease interaction with Fib. Therefore, the Fib adsorption resistance of PEG-modified surface depended on the grafting density of PEG layer and the deformation capacity of the PEG chain.

Acknowledgements

The authors acknowledge the financial support of the National Natural Science Foundation of China (Project nos 51303178 and 21274150).

References

1 A. Monkawa, T. Ikoma, S. Yunoki, T. Yoshioka, J. Tanaka, D. Chakarov and B. Kasemo, *Biomaterials*, 2006, **27**, 5748–5754.
2 G. B. Sigal, M. Mrksich and G. M. Whitesides, *J. Am. Chem. Soc.*, 1998, **120**, 3464–3473.
3 S. Y. Jung, S. M. Lim, F. Albertorio, G. Kim, M. C. Gurau, R. D. Yang, M. A. Holden and P. S. Cremer, *J. Am. Chem. Soc.*, 2003, **125**, 12782–12786.
4 A. Toscano and M. M. Santore, *Langmuir*, 2006, **22**, 2588–2597.
5 Z. Bai, M. Filiaggi and J. Dahn, *Surf. Sci.*, 2009, **603**, 839–846.
6 Y. F. Yano, *J. Phys.: Condens. Matter*, 2012, **24**, 503101–503117.
7 C. F. Wertz and M. M. Santore, *Langmuir*, 2001, **17**, 3006–3016.
8 J. Jin, W. Jiang, J. Yin, X. Ji and P. Stagnaro, *Langmuir*, 2013, **29**, 6624–6633.
9 A. Bratek-Skicki, P. Żeliszewska, Z. Adamczyk and M. Cieśla, *Langmuir*, 2013, **29**, 3700–3710.
10 Z. Adamczyk, A. Bratek-Skicki, P. Dąbrowska and M. Nattich-Rak, *Langmuir*, 2011, **28**, 474–485.
11 K. Bergström, K. Holmberg, A. Safranj, A. S. Hoffman, M. J. Edgell, A. Kozlowski, B. A. Hovanes and J. M. Harris, *J. Biomed. Mater. Res.*, 1992, **26**, 779–790.
12 F. J. Xu, Y. L. Li, E. T. Kang and K. G. Neoh, *Biomacromolecules*, 2005, **6**, 1759–1768.
13 J. Narayanan and X. Y. Liu, *Biophys. J.*, 2003, **84**, 523–532.
14 C. Sacchetti, K. Motamedchaboki, A. Magrini, G. Palmieri, M. Mattei, S. Bernardini, N. Rosato, N. Bottini and M. Bottini, *ACS Nano*, 2013, **7**, 1974–1989.
15 L. D. Unsworth, H. Sheardown and J. L. Brash, *Biomaterials*, 2005, **26**, 5927–5933.
16 L. D. Unsworth, H. Sheardown and J. L. Brash, *Langmuir*, 2005, **21**, 1036–1041.
17 K. E. Bremmell, L. Britcher and H. J. Griesser, *Colloids Surf., B*, 2013, **106**, 102–108.
18 T. Riedel, Z. Riedelova-Reicheltova, P. Majek, C. Rodriguez-Emmenegger, M. Houska, J. E. Dyr and E. Brynda, *Langmuir*, 2013, **29**, 3388–3397.
19 L. M. Pandey, S. K. Pattanayek and D. Delabouglise, *J. Phys. Chem. C*, 2013, **117**, 6151–6160.
20 S. J. Sofia, V. Premnath and E. W. Merrill, *Macromolecules*, 1998, **31**, 5059–5070.
21 K. E. Sapsford and F. S. Ligler, *Biosens. Bioelectron.*, 2004, **19**, 1045–1055.
22 K. A. Marx, *Biomacromolecules*, 2003, **4**, 1099–1120.
23 T. Wang, X. Wang, Y. Long, G. Liu and G. Zhang, *Langmuir*, 2013, **29**, 6588–6596.
24 Y. Arima and H. Iwata, *Biomaterials*, 2007, **28**, 3074–3082.
25 J. D. Moore, M. A. Perez-Pardo, J. F. Popplewell, S. J. Spencer, S. Ray, M. J. Swann, A. G. Shard, W. Jones, A. Hills and D. G. Bracewell, *Biosens. Bioelectron.*, 2011, **26**, 2940–2947.
26 P. D. Coffey, M. J. Swann, T. A. Waigh, Q. Mu and J. R. Lu, *RSC Adv.*, 2013, **3**, 3316–3324.
27 F. Evers, K. Shokuie, M. Paulus, C. Sternemann, C. Czeslik and M. Tolan, *Langmuir*, 2008, **24**, 10216–10221.
28 I. Reviakine, D. Johannsmann and R. P. Richter, *Anal. Chem.*, 2011, **83**, 8838–8848.
29 P. Xu, F. Huang and H. Liang, *Biosens. Bioelectron.*, 2013, **41**, 505–510.
30 T. J. Zwang, R. Patel, M. S. Johal and C. R. Selassie, *Langmuir*, 2012, **28**, 9616–9620.
31 M. Westwood, T. R. Noel and R. Parker, *Carbohydr. Polym.*, 2013, **94**, 137–146.
32 S. Forbes, A. J. McBain, S. Felton-Smith, T. A. Jowitt, H. L. Birchenough and C. B. Dobson, *Biomaterials*, 2013, **34**, 5453–5464.
33 K. Xu, M. M. Ouberai and M. E. Welland, *Biomaterials*, 2013, **34**, 1461–1470.
34 W. Kern, *RCA rev.*, 1970, **31**, 187–206.
35 K. H. Choi, J. M. Friedt, W. Laureyn, F. Frederix, A. Campitelli and G. Borghs, *J. Vac. Sci. Technol., B*, 2003, **21**, 1433–1436.
36 A. G. Hemmersam, M. Foss, J. Chevallier and F. Besenbacher, *Colloids Surf., B*, 2005, **43**, 208–215.
37 N. Weber, H. P. Wendel and J. Kohn, *J. Biomed. Mater. Res., Part A*, 2005, **72**, 420–427.
38 L. Palmqvist and K. Holmberg, *Langmuir*, 2008, **24**, 9989–9996.

39 S. Slavin, A. H. Soeriyadi, L. Voorhaar, M. R. Whittaker, C. R. Becer, C. Boyer, T. P. Davis and D. M. Haddleton, *Soft Matter*, 2012, **8**, 118–128.
40 A. K. Dutta, A. Nayak and G. Belfort, *J. Colloid Interface Sci.*, 2008, **324**, 55–60.
41 A. Domack, O. Prucker, J. Rühe and D. Johannsmann, *Phys. Rev. E: Stat. Phys., Plasmas, Fluids, Relat. Interdiscip. Top.*, 1997, **56**, 680.
42 M. V. Voinova, M. Rodahl, M. Jonson and B. Kasemo, *Phys. Scr.*, 1999, **59**, 391.
43 F. Höök, J. Vörös, M. Rodahl, R. Kurrat, P. Böni, J. Ramsden, M. Textor, N. Spencer, P. Tengvall and J. Gold, *Colloids Surf., B*, 2002, **24**, 155–170.
44 J. Malmstrom, H. Agheli, P. Kingshott and D. S. Sutherland, *Langmuir*, 2007, **23**, 9760–9768.
45 F. Huang and H. Liang, *ACS Appl. Mater. Interfaces*, 2013, **5**, 5025–5033.
46 J. DeFeijter, d. J. Benjamins and F. Veer, *Biopolymers*, 1978, **17**, 1759–1772.
47 S. Alexander, *J. Phys.*, 1977, **38**, 983–987.
48 L. D. Unsworth, Z. Tun, H. Sheardown and J. L. Brash, *J. Colloid Interface Sci.*, 2005, **281**, 112–121.
49 H. Hähl, F. Evers, S. Grandthyll, M. Paulus, C. Sternemann, P. Loskill, M. Lessel, A. K. Hüsecken, T. Brenner and M. Tolan, *Langmuir*, 2012, **28**, 7747–7756.
50 G. Zhang and C. Wu, *Macromol. Rapid Commun.*, 2009, **30**, 328–335.
51 Y. Inoue, T. Nakanishi and K. Ishihara, *Langmuir*, 2013, **29**, 10752–10758.
52 M. Bergkvist, J. Carlsson and S. Oscarsson, *J. Biomed. Mater. Res.*, 2003, **64**, 349–356.
53 L. Renner, T. Pompe, K. Salchert and C. Werner, *Langmuir*, 2005, **21**, 4571–4577.

